Thermoelastic behavior of X-ray lithography masks during irradiation

by I. A. Shareef
J. R. Maldonado
Y. Vladimirsky
D. L. Katcoff

This paper presents computer calculations of thermoelastic effects in X-ray lithography masks caused by the absorption of X-rays during exposure. Several mask structures are considered, with different substrate and absorber materials, using finite element analysis. Part I of the paper deals with short-pulse X-ray irradiation (e.g., from gas plasma, laser-heated plasma, or exploding wire sources), and Part II describes irradiation during exposure with a synchrotron-storage-ring X-ray source. For the short-pulse irradiation, results indicate a maximum rise in temperature on the mask of about 30°C for a 2-ns exposure with a 10-mJ/cm^2 X-ray pulse. Mechanical static analysis shows that the maximum stress in the absorber films, which is due to maximum temperature differences in the mask layers, occurs at the end of the pulse. The magnitude of the induced thermoelastic stress is found comparable to the intrinsic stress level of the mask materials (typically 2–5 × 10^8 dyn/cm^2). The analysis indicates that when pulse amplitudes reach 10 mJ/cm^2, there will be a need for experimental study of X-ray mask distortion during exposure to short X-ray pulses. A one-dimensional model is developed for the case of storage-ring irradiation. The model predicts distortions of the printed image due to a thermal wave developed on the mask by scanning of the X-ray beam. Experimental results are presented showing that the effect is negligible under normal operating conditions but may become noticeable for operation in vacuum or without proper heat sinks.

©**Copyright** 1990 by International Business Machines Corporation. Copying in printed form for private use is permitted without payment of royalty provided that (1) each reproduction is done without alteration and (2) the *Journal* reference and IBM copyright notice are included on the first page. The title and abstract, but no other portions, of this paper may be copied or distributed royalty free without further permission by computer-based and other information-service systems. Permission to *republish* any other portion of this paper must be obtained from the Editor.

Introduction

This paper presents computer simulations of the thermoelastic behavior of X-ray lithography masks during X-ray exposure. The results were obtained using commercially available finite element analysis programs

(NASTRAN[1] and CAEDS[2]). In its simplest structure, shown in **Figure 1**, an X-ray lithography mask consists of an X-ray-transparent substrate coated with a patterned metallic X-ray absorber. The mask is irradiated from the substrate side to replicate the pattern on a resist-coated wafer. Mask heating during X-ray lithography exposure using proximity printing is of concern, since it may cause pattern displacements (mask distortion) and mechanical failure due to stresses that may be developed in the mask substrate and absorber.

Two kinds of X-ray exposure situations are considered in this paper. In Part I, the X-ray mask is subjected to short, intense X-ray pulses (e.g., from a plasma source, a laser-heated plasma X-ray source, or an exploding wire source). In Part II, the X-ray lithography is performed using a scanning beam from a synchrotron-storage-ring source. A theoretical calculation is presented using a one-dimensional model predicting heat-wave-like deformations of the mask and the printed image.

The studies presented here shed light on the feasibility of reducing thermoelastic effects, which cause distortion and reduce lifetime in X-ray lithography masks.

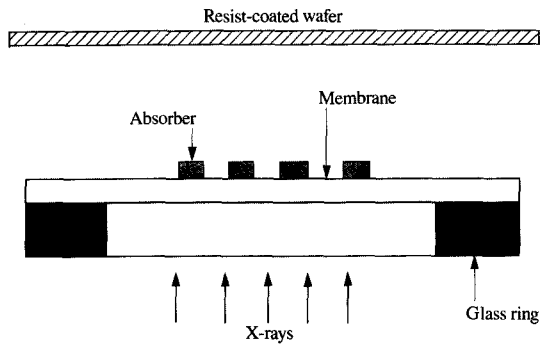

Figure 1

X-ray mask structure.

I. Short-pulse irradiation

X-ray lithography using short X-ray pulses generated from hot plasmas is an area of great interest because of the possibility of realizing, relatively inexpensively, an alternative to a storage-ring X-ray source [1]. The thermal and mechanical behavior of X-ray masks under pulse heating has been studied by Ballantyne et al. [2] and Hyman et al. [3], using both a theoretical model and a finite element analysis program. Their results are in relatively good agreement with the more complete computer simulations presented in this paper and others [4–6] previously published by us.

• *Model for short-pulse irradiation*

A microscopic model with adiabatic boundary conditions is used for the heat calculations. The mask consists of identical rectangular sections 2 μm thick by 5 × 7 μm. The model used for each mask section is shown in **Figure 2**. The finite element model is constructed, for multiple material layers, using CAEDS. To simplify the calculations, we divide the mask substrate into two layers of elements. Furthermore, the incident X-ray flux is assumed to be absorbed uniformly by the mask substrate. This is a reasonable assumption, since for example the Si substrate absorbs only about 23% of the incident X-ray flux at 8.3 Å. The absorber pattern used in the

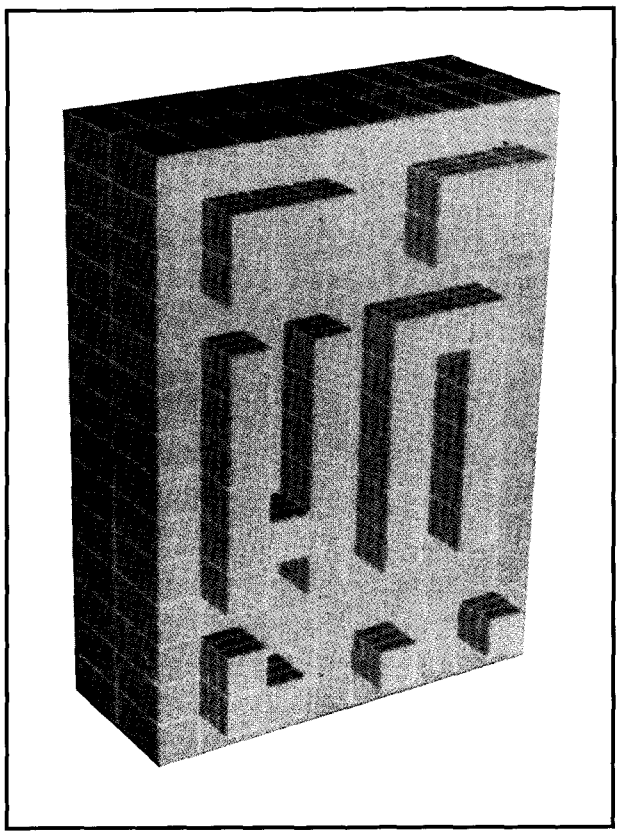

Figure 2

Model used in the calculations. A mask substrate section 5 μm × 7 μm with Au absorber elements is shown. The Au features are formed by 0.5-μm-square elements 0.2 μm thick.

[1] NASTRAN is a trademark of MacNeal-Schwendler Corporation, 815 Colorado Blvd., Los Angeles, CA 90041.

[2] CAEDS is a registered trademark of International Business Machines Corporation.

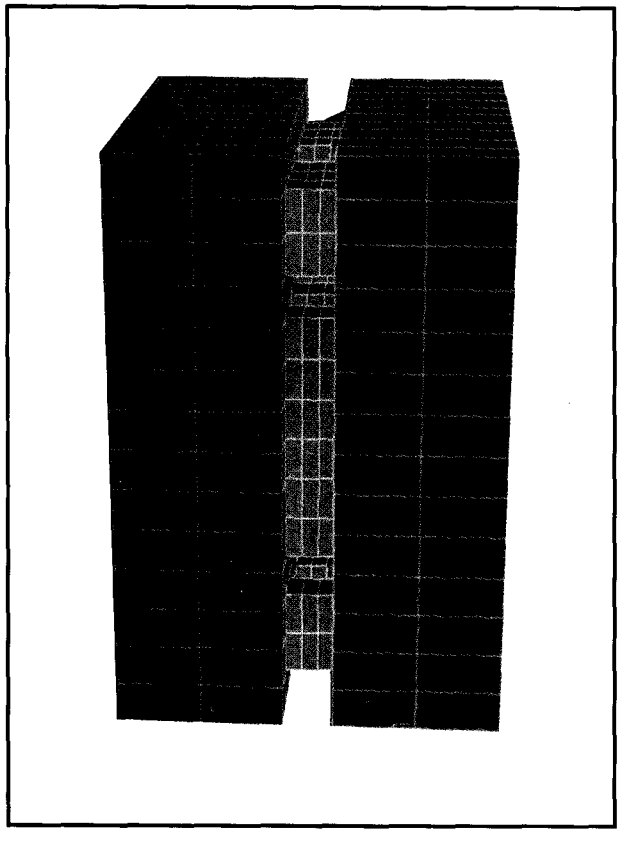

Figure 3

Model used in the calculations. The absorber is shown sandwiched between the substrate (left) and the He (right). As explained in the text, the He layer is shown with a thickness of 2 μm instead of the 40-μm thickness actually used.

calculations consists of several lines and pads comprising three layers of finite elements. Each layer is 0.2 μm thick and is made up of 0.5-μm-square elements. The absorber/substrate coverage is about 30% (typical of some lithographic levels). Calculations using 100% coverage are also performed, and the temperatures are found not to differ appreciably from the hottest areas of the 30% coverage case. Again, to simplify the calculations, each absorber layer is assumed to absorb the incident X-ray flux uniformly. The absorption in each layer is calculated from the known absorption coefficients of the absorber materials. For the Au absorber, the calculated total absorption of the three layers is 94% of the X-ray flux at the incident wavelength of 8.3 Å. All the absorbed energy is assumed to be converted into heat, which is assumed to be conducted to the mask substrate or through the He gas. (The exposures are conducted in a He atmosphere to reduce the rise in temperature of the mask.) The heat loss by radiation, which may be dominant during the length of the X-ray pulse, is neglected because of uncertainties in the emissivity of the mask components. In addition, energy transformed into thermoelastic waves is also neglected. These assumptions may lead to higher predicted temperatures and may cause an underestimation of the value of the maximum X-ray-pulse amplitude that a given mask structure can withstand due to thermoelastic effects.

It is desired to model a gap of 40 μm (typical for proximity printing) filled with He at atmospheric pressure between the mask and the wafer, which is held at room temperature. To reduce the number of elements, and therefore decrease the required CPU time, a 2-μm He gap is used instead of the actual 40-μm gap, and the thermal conductivity of He is scaled down by a factor of 20 in the direction perpendicular to the plane of the mask, to compensate for the smaller gap. The scaled thermal conductivity and He gap in the model yield the same thermal resistance as the real 40-μm gap. The model with the He layer is shown in **Figure 3**.

The values used in the calculations for the thermal and mechanical parameters of the different materials are shown in **Table 1**. An X-ray pulse with total energy of 10 mJ/cm^2 is assumed to be incident on the mask in all cases treated below. That total pulse energy is beyond the reach of today's plasma sources for X-ray lithography applications, but it is representative of what may be needed in a system with high wafer throughput.

The microscopic model described above is also used for the thermal stress calculations. The 5 × 7-μm mask structure is assumed to be free of intrinsic stress (in normal operation, a mask is typically under a tension of 5×10^8 dyn/cm^2). This assumption is justified, since for mask fatigue considerations we are mainly interested in the stress at the interface between the absorber features and a Si or polyimide substrate. The global distortions (distortions over large distances) induced by the thermal stresses are not calculated in this microscopic model. However, for a uniform illumination of the whole surface of the X-ray mask (as from a plasma X-ray source), global distortions are expected to be small as long as the induced thermal stress does not change the mask substrate stress locally from tensile to compressive. This criterion is used below to estimate the maximum allowed pulse amplitude. Von Mises stress values are obtained for different mask structures and different pulse lengths. Von Mises stress is the root mean square value of the six components of stress (three components each of normal and shear stress) and is considered to be representative of the actual stress on the structure. The results for nonuniform illumination (storage-ring irradiation) are shown in Part II.

Table 1 Thermomechanical parameters.

	Poisson ratio, ν	*Thermal conductivity, κ* (W/cm-°C)	*Thermal expansion, α* ($\times 10^{6}$)	*Young's modulus, E* ($\times 10^{-12}$ dyn/cm^2)	*Thickness, t* (μm)	*Density, d* (g/cm^3)	*X-ray mass absorption coefficient at 8.3 Å, μ* (cm^2/g)
Si	0.279	1.49	2.3	1.3	2	2.3	543
Au	0.33	3.15	14.2	0.74	0.6	19.6	2305
W	0.4	1.78	4.5	3.45	0.6	19.3	1776
He		0.0014			40		16.8
Ta	0.4	0.54	6.5	1.86	0.6	16.6	1688
C	0.07	6.55	1.2	11.2	2	3.2	718
SiC	0.27	0.41	2.3	3.8	2	3.21	643

Table 2 Thermoelastic effects.

Mask type	$\lambda = 8.3$ *Å*		$\lambda = 10$ *Å*	
	Maximum rise in temperature, δT (°C)	*Maximum Von Mises stress, σ* (dyn/cm^2 $\times 10^{-8}$)	*Maximum rise in temperature, δT* (°C)	*Maximum Von Mises stress, σ* (dyn/cm^2 $\times 10^{-8}$)
Si–Au	31.80	2.80	30.46	2.68
Si–Ta	*	*	36.10	2.80
Si–W	28.00	2.00	30.40	1.98
SiC–Au	29.70	3.05	24.27	2.30
SiC–W	26.70	2.50	25.60	2.15
SiC–Ta	*	*	29.38	2.76
C–Au	21.52	2.7	18.01	1.60

The following parameters are fixed for all calculations: mask structure, as described in text; pulse energy = 10 mJ/cm^2; pulse length = 2 ns.
* Not calculated.

• *Calculations for short-pulse irradiation*

Several mask structures consisting of different substrate and absorber materials are considered. The results are summarized in **Table 2**, for two X-ray wavelengths of interest in X-ray lithography, and are discussed in detail in the following sections. Color graphic representations of the temperature and stress distribution in the X-ray mask at times during and after the application of the X-ray pulse are also presented.

Si–Au mask structure

Computer simulations are performed for an X-ray mask with a Si substrate and a Au absorber. As mentioned previously, all the substrate materials are 2 μm thick and the absorber films 0.6 μm thick. In practice, the thickness of the substrate and absorber may differ for different materials. Incident X-ray pulses with total energy of 10 mJ/cm^2 and various lengths (2, 5, 10, 20 and 30 ns) are used in the calculations, for two different X-ray wavelengths. **Figure 4** is a contour plot of the temperature distribution on the mask for the Si–Au mask structure at the end of a 2-ns pulse with 8.3-Å wavelength. This plot is similar to the results obtained for all the mask structures studied. One can see in the figure that the maximum temperature of 31.6°C occurs at the Au features that are closer together on the Si substrate. Calculations for the case of 100% coverage indicate a maximum rise in temperature very close to the maximum encountered in the 30% coverage case. Heat transfer between the Au features can also be seen. The temperature range between the hottest and coolest Au features is about 6°C for the 30% Au coverage used in our calculations. One can also see that the calculated temperature is very uniform through the thickness of the Au absorber because of the good thermal conductivity of Au.

The response of the mask as a function of time to pulses of various lengths and 8.3-Å wavelength is shown in **Figure 5**. For each pulse length, the figure shows the temperature (calculated at a Au feature of the mask where the maximum rise in temperature was calculated) vs. time. It is observed from the figure that for all the pulse lengths, the maximum rise in temperature occurs at the completion of the X-ray pulse. The temperature then decays exponentially with a time constant determined by the conduction of heat from the Au to the Si substrate.

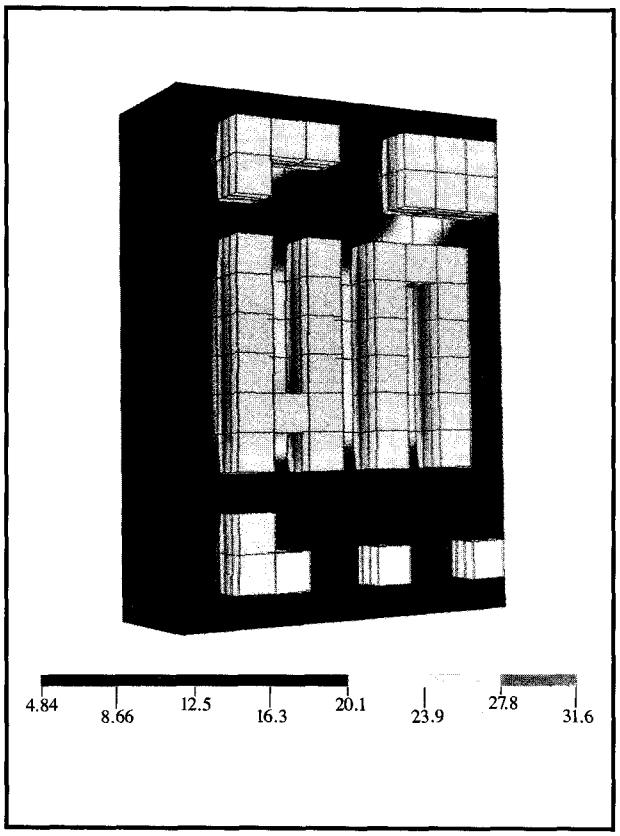

Figure 4

Thermal distribution of an X-ray-irradiated Si–Au mask at the end of a 2-ns pulse of 8.3 Å and 10 mJ/cm^2 total energy. The brighter areas indicate higher temperatures (temperature values in °C).

After this, the temperature remains fairly constant until heat conduction through the He gas to the heat sink becomes appreciable. Figure 5 shows that for all pulse lengths, the mask reaches the initial ambient temperature after about 10 ms. This indicates that it is possible to operate under the assumed conditions with a 100-Hz repetition rate for 10-mJ/cm^2 pulses without causing any appreciable average heating in the mask. Figure 5 also shows that the maximum temperature increases as the pulse length is decreased; this is because the peak power increases with decreasing pulse length for a given total X-ray pulse energy.

The time dependence of the calculated temperature on the Si substrate due to a 20-ns X-ray pulse is shown in **Figure 6** for two locations, one on the absorber side next to a Au feature, and one inside the substrate (halfway through the thickness). The temperature of the first location shows a relative maximum at the end of the pulse due to the influence of the adjacent Au features. The temperature of the second location shows an essentially monotonic increase during the pulse and then stabilizes until the heat is conducted away by the He gas toward the heat sink (wafer).

The thermoelastic results for the Si–Au mask structure are shown in **Figure 7** for the Von Mises stress at the end of a 2-ns pulse. It can be seen from Figure 7 that the stress is maximum (2.8×10^8 dyn/cm^2) inside the Au absorber, close to the Si–Au interface. As the interface is approached, the stress becomes slightly lower. The highest calculated stress is somewhat lower than the intrinsic stress in the substrate and absorber of present-day X-ray masks, and if the pulse energy is increased

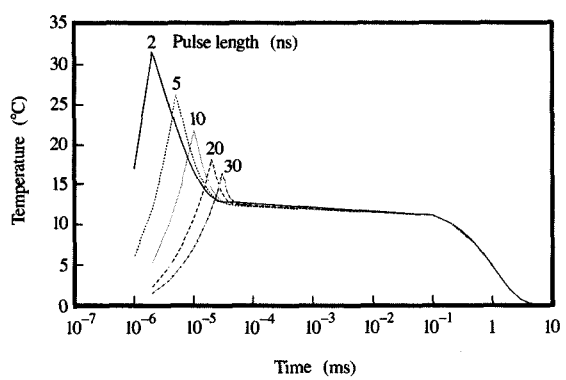

Figure 5

Calculated temperature vs. time at a Au feature of a Si–Au mask structure for 2-, 5-, 10-, 20-, and 30-ns pluses of 8.3-Å wavelength.

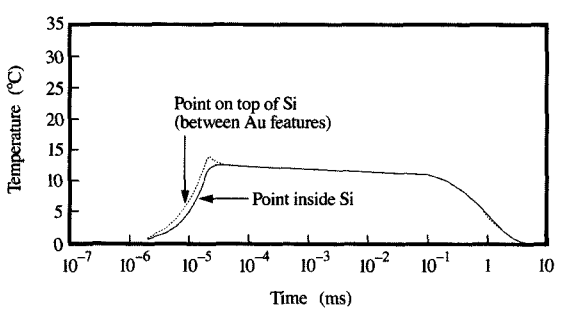

Figure 6

Calculated temperature vs. time for two points on the Si substrate of a Si–Au structure for 2-ns pulses of 8.3-Å wavelength and 10 mJ/cm^2 total energy. One point is adjacent to a Au feature; the other point is in the middle of the Si substrate (halfway through the thickness).

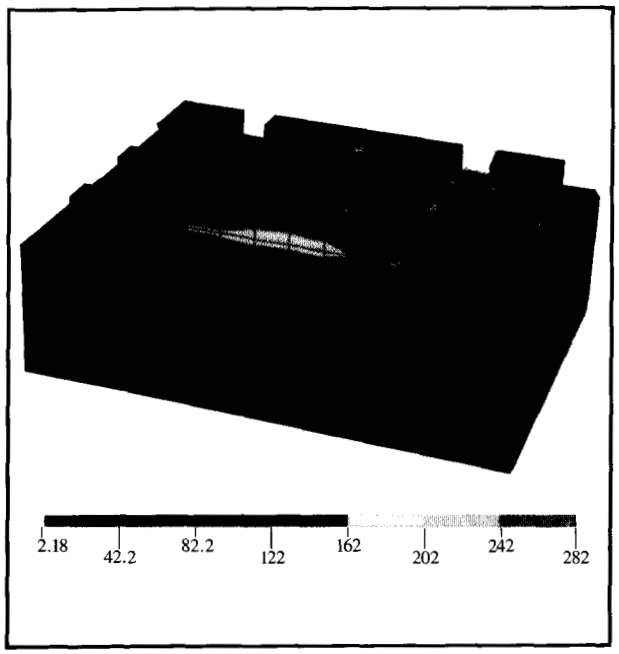

Figure 7

Thermally induced Von Mises stress on X-ray mask at the end of a 2-ns X-ray pulse of 8.3-Å wavelength for a Si–Au mask structure (stress values in dyn/mm^2 × 10^4).

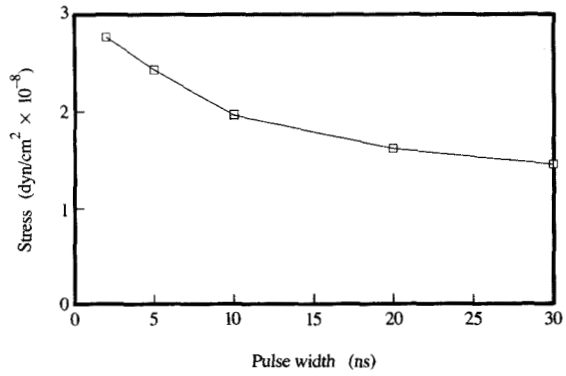

Figure 8

Dependence of stress (at the absorber–Si substrate interface) on pulse width for a Si–Au structure. Pulse has 10 mJ/cm^2 total energy and 8.3-Å wavelength.

until the induced stress overcomes the intrinsic stress of the substrate, large global mask distortions may occur. Subject to experimental verification, it is reasonable to assume that with the use of X-ray pulses higher than 10 mJ/cm^2, thermal cycling may lead to unwanted distortions and mask fatigue problems. **Figure 8** shows that the stress values decrease with increasing pulse length, as expected from the calculated temperature distributions shown above. For a pulsed X-ray source, the maximum length of the pulse may be limited by X-ray production efficiency considerations in the X-ray target. Therefore, the use of long pulses to decrease the induced stress may not be possible.

Si–polyimide mask structure

Organic films such as polyimide (PI) are currently used in some X-ray mask structures for reasons that include ease of mask handling and optical alignment. For the Si–PI case, the calculations are performed with a mask structure consisting of a 1-μm-thick Si membrane coated with a 1-μm-thick polyimide film with a Au absorber on top. The temperature distribution in the mask after a 20-ns pulse is shown in **Figure 9**. The maximum rise in temperature at the Au absorber is 30.8°C. The time dependence of the temperature calculated in a Au feature

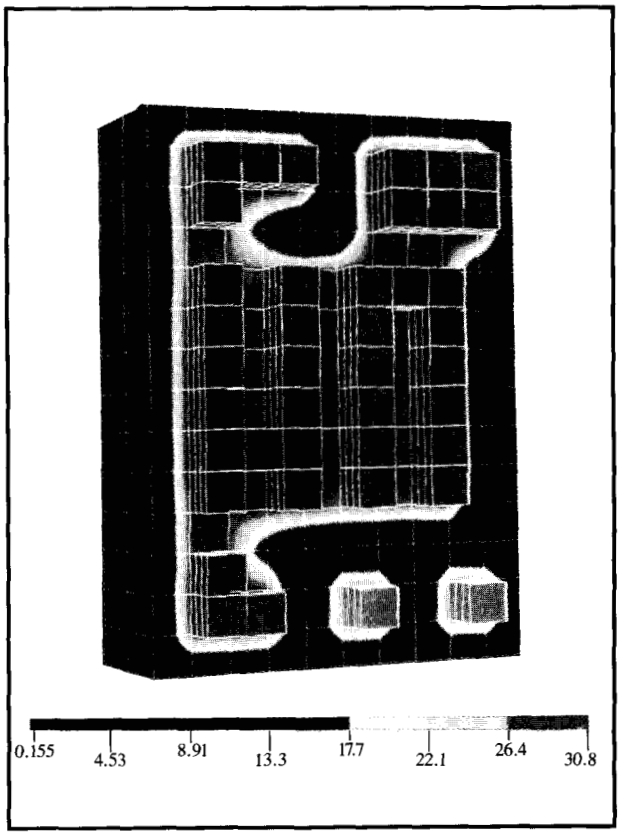

Figure 9

Thermal distribution of Si–PI X-ray mask after a 20-ns pulse of 8.3-Å wavelength and 10 mJ/cm^2 total energy, calculated at a Au feature on an X-ray mask consisting of a 1-μm Si membrane coated with a 1-μm PI film (temperature values in °C).

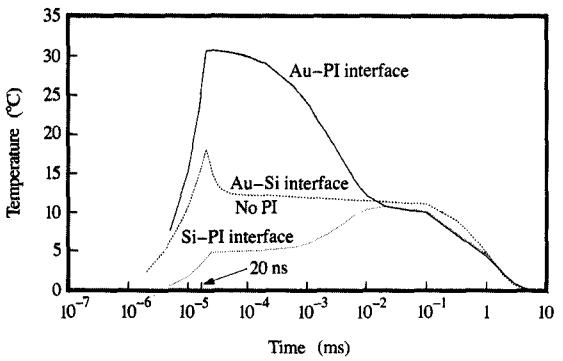

Figure 10

Thermal response of X-ray mask with Si–PI–Au structure compared with that of a Si–Au mask structure. On the Si–PI–Au mask, two points are shown, one at the Au–PI absorber interface, and the other at the Si–PI interface. The point on the Si–Au mask is in the Au absorber.

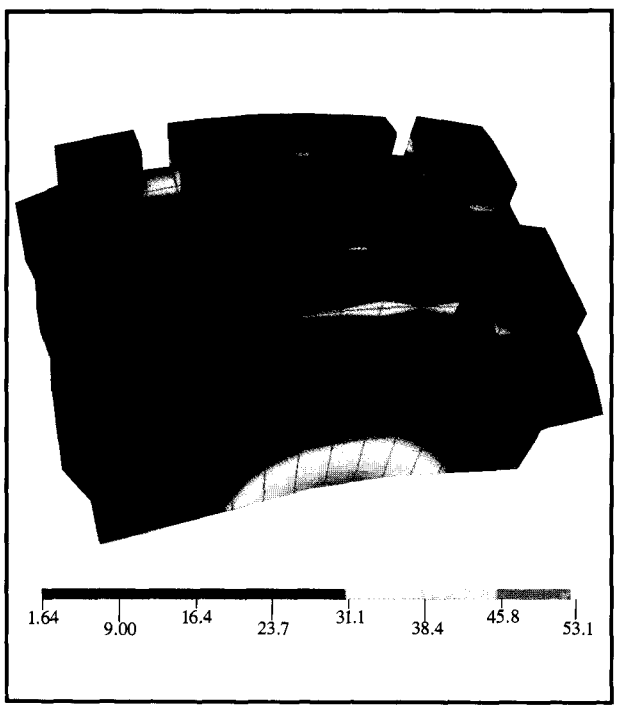

Figure 11

Thermally induced Von Mises stress on X-ray mask at the end of a 20-ns X-ray pulse of 8.3-Å wavelength for a Si–PI structure (stress values in dyn/mm^2 × 10^4). The deformation of the structure is shown magnified 300×.

on the PI film is shown in **Figure 10** for a 20-ns pulse. The calculated results in a Au feature for a 20-ns pulse on a Si–Au structure are also shown for comparison in Figure 10 (that curve also appears in Figure 5). The figure shows that the presence of the PI film increases the maximum temperature in the Au absorber by about 13°C, relative to the case without PI. The figure also shows that the temperature in the Au feature on the PI film remains relatively high after the completion of the 20-ns pulse until about 0.01 ms after the start of the pulse, in contrast to the Si–Au case. This is due to the low thermal capacity of the PI film, which delays heat conduction from the Au feature to the Si substrate. About 0.01 ms after the start of the pulse (a delay determined by the thermal conduction properties of the PI film), the temperature in the Au feature decreases to about 11°C. After about 0.1 ms, the temperature in the Au feature starts to decrease, due to conduction by the He gas to the heat sink (wafer). This interpretation is supported by results, shown in Figure 10, for the time dependence of the temperature calculated at the Si–PI interface. The figure shows that the temperature at a point on the Si–PI interface increases after the completion of the 20-ns X-ray pulse until it reaches a plateau at about 30 ns. (Since there are two sources of heat, the mask substrate and the Au absorber, the net effect is a longer time to reach the first plateau.) It is also observed that during the same interval, the temperature of a point on the Au absorber–PI interface decreases. Both points reach the same temperature (11°C) after about 0.01 ms. This indicates that heat is being transferred through the polyimide into the Si, and thermal equilibrium is eventually reached.

It is known that the thermal expansion of PI films is anisotropic and depends on the particular PI composition. Therefore, to obtain more general results, the stress calculations for the Si–PI mask structure are performed for two cases with different values of the thermal expansion of the polyimide film, which is assumed to be isotropic in both cases. In one case, the thermal expansion coefficient is set to the lowest measured value in the plane of the film for the PI composition (22×10^{-6}). In the other case, the thermal expansion coefficient is set to the average of the in-plane and out-of-plane values (66×10^{-6}). The results for the first case are shown in **Figure 11**. It is observed that the maximum stress (5.3×10^7 dyn/cm^2) in the absorber occurs at the Au–PI interface. This value is about one-fourth the maximum stress in the case described above of the mask structure without polyimide. For a thermal expansion of 66×10^{-6} (the second case), the resulting maximum stress at the interface is 1.87×10^8 dyn/cm^2. This value is comparable to the corresponding one calculated for the mask structure without PI. Therefore,

depending on the particular PI film and its deposition conditions, its use as an intermediate layer may or may not produce an appreciable change of the stress during irradiation, compared to mask structures without polyimide films.

Si–W mask structure

The results of the calculations of rise in temperature for the Si–W mask structure (with the same geometry as the Si–Au structure) are shown in **Figure 12** for a 0.6-μm W absorber on a 2-μm Si substrate for a 2-ns pulse of 8.3-Å wavelength. The maximum rise in temperature in the W film is about 28°C (somewhat lower than the case of the Au absorber, because of the lower X-ray absorption of the W film). The figure also shows that there is a temperature gradient through the thickness of the W features due to the relatively lower thermal conductivity of W when compared with Au.

The stress calculations for the Si–W mask structure for a 2-ns pulse, shown in **Figure 13**, indicate that the

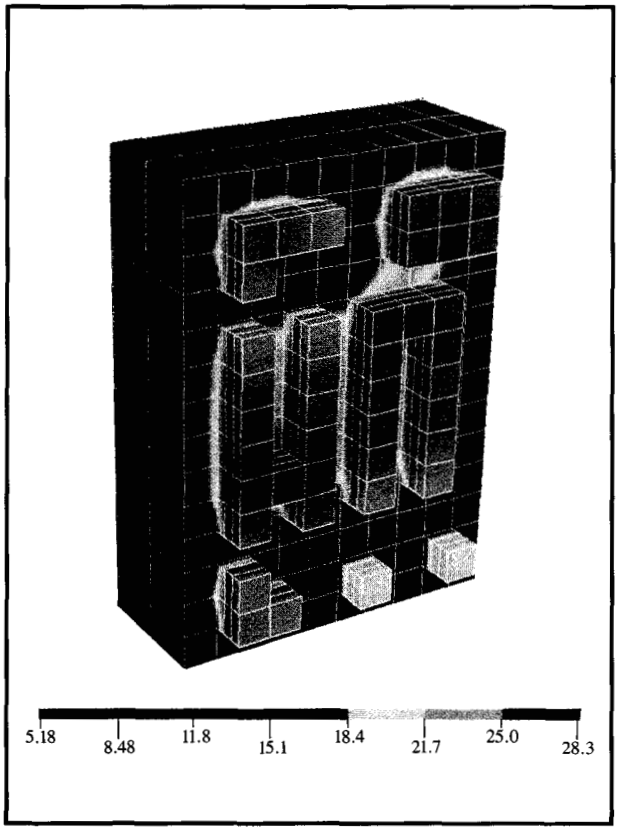

Figure 12

Thermal distribution on an X-ray mask with Si–W structure after a 2-ns, 10-mJ/cm^2 X-ray pulse of 8.3-Å wavelength (temperature values in °C).

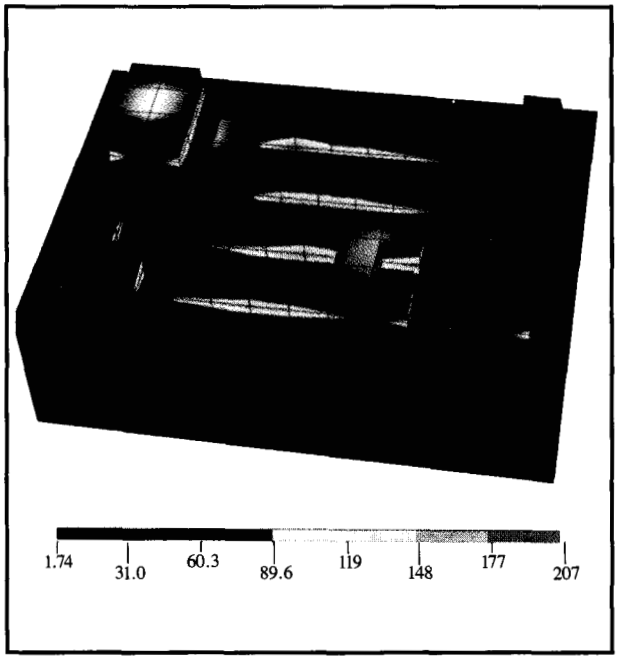

Figure 13

Thermally induced Von Mises stress on a Si–W X-ray mask at the end of a 2-ns pulse of 8.3-Å wavelength for a Si–W structure (stress values in dyn/mm^2 × 10^4).

maximum stress at the Si–W interface is 2.07×10^8 dyn/cm^2 (about 30% lower than the calculated value for the case of a Au absorber). This is a surprising result, since we would have expected a much lower stress value due to the better matching of the thermal expansion coefficients of Si and W. The unexpected result may be attributed to the fact that W has a larger value of Young's modulus than Au (about five times greater), as shown in Table 1.

Si–Ta mask structure

Because of space limitations, the figures for this case and the following have been omitted. The maximum rise in temperature in this structure for a 2-ns X-ray pulse at 10 Å is 36.1°C and is the largest of all the materials studied. This may be attributed to the relatively low thermal conductivity of Ta. The Von Mises stress simulations indicate a maximum value of 2.80×10^8 dyn/cm^2. This relatively large value may be attributed to the difference in thermal expansion between Si and Ta. It is interesting to note that the stress in Au, despite an even larger mismatch with Si, is comparable when Si substrates are used. This is due to the relatively high Young's modulus of Ta and its low thermal conductivity (lower than W). The lack of good heat dissipation creates a severe thermal gradient through the thickness of the Ta absorber film. Since Ta films thicker than 0.6 μm will be required in

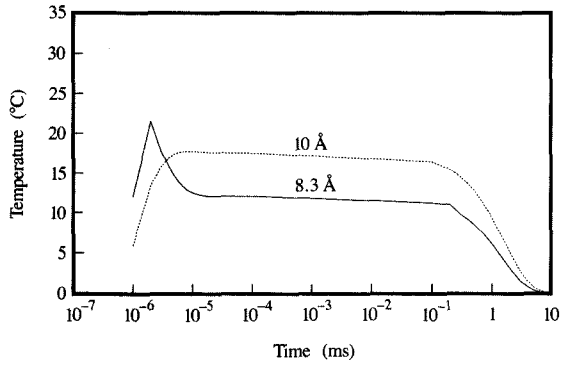

Figure 14

Rise in temperature at a point on the Au absorber where the rise in temperature is maximum vs. time, for a diamond–Au X-ray mask at two different wavelengths.

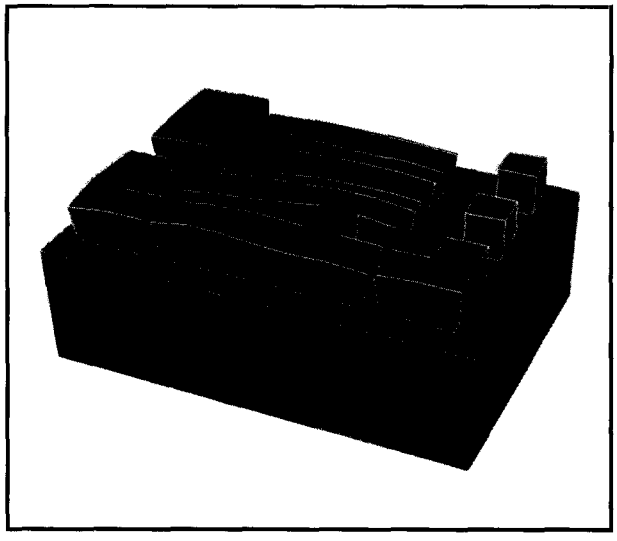

Figure 15

Thermal distortion of diamond–Au X-ray mask (2-ns, 8.3-Å-wavelength X-ray pulse). The graph has been magnified (1000×) to show the effect of the larger expansion of Au relative to diamond. The maximum displacement of the Au absorber is about 1 ppm.

order to achieve adequate mask contrast, no stress improvement is expected. Therefore, the thermoelastic effects on Si–Ta and SiC–Ta structures at 8.3 Å are not calculated in this paper.

SiC–Au mask structure

For a 2-ns pulse at 8.3 Å on a SiC–Au mask, the maximum rise in temperature is 29.7°C. The corresponding Von Mises stress has a maximum value of 3.05×10^8 dyn/cm^2 because of the large thermal expansion mismatch between SiC and W. Both temperature increase and stress are reduced with operation at a longer wavelength (10 Å), as shown in Table 2.

SiC–W mask structure

The thermal response of this structure and the Von Mises stress are shown in Table 2. It is observed from Table 2 that the maximum rise in temperature and corresponding maximum Von Mises stress are reduced somewhat from the case of the SiC–Au mask structure. The reductions, however, are not as large as might be expected based on thermal expansion matching between W and Si, because of the poor thermal conductivity of W.

SiC–Ta mask structure

The thermoelastic results for this structure are also shown in Table 2. The calculations were performed only at a wavelength of 10 Å.

Diamond(C)–Au mask structure

The results for this structure for 10-Å and 2-ns X-ray pulses are presented in Table 2. For pulses of 10-Å wavelength, the diamond–Au structure offers some advantages. **Figure 14** shows the thermal response of a diamond–Au X-ray mask for X-ray pulses of 8.3-Å and 10-Å wavelengths. For the 10-Å case, there is no appreciable peak in temperature at the Au features on the mask. Therefore, the temperature difference between the Au and the diamond substrate is reduced, and the induced stress is also considerably decreased compared to its value for 8.3 Å, as observed from Table 2. For the 8.3-Å wavelength, the maximum temperature calculated for the diamond substrate is about 70% of that of the other two substrates. However, the maximum calculated value for the Von Mises stress of the diamond–Au mask structure is relatively high (3.05×10^8 dyn/cm^2), as shown in Table 2 (which is about the same as the intrinsic stress of the substrate and absorber materials). The large induced stress is due to the large difference in the thermal expansion coefficient of the two materials. The stress can be seen in **Figure 15**, where the expansion of the Au absorber on the diamond substrate has been magnified.

- *Performing mask irradiation with short X-ray pulses: System considerations*

Effect of X-ray wavelength on the mask thermal behavior

Figure 16 shows the calculated temperature vs. time at a Au feature for an X-ray mask with a Si substrate, for two different wavelengths. The maximum rise in temperature

of the mask absorber occurs at the end of the pulse and is slightly higher for the pulse with the short wavelength. However, after the completion of the 2-ns pulse, the calculated temperature of the Au feature is higher for the 10-Å X-ray pulse. This behavior is explained by the greater X-ray absorption of the Si substrate at the longer wavelength. For both wavelengths, most of the incident X-ray energy from the substrate is absorbed by the Au. A similar behavior is observed from Table 2 for the W absorber on a SiC substrate at the two wavelengths, and differs from the case of the Au absorber due to the lower thermal conductivity of W. The thermoelastic effects in the diamond–Au structure, discussed above, indicate that the 10-Å wavelength is advantageous for this particular structure.

Effect of substrate material for Au absorber

The calculated temperature (for 8.3-Å X-ray pulses) at a Au feature on the mask is shown in **Figure 17** for three different substrate materials 2 μm thick. The Si and SiC substrates present essentially the same behavior. However, the maximum calculated temperature at the Au absorber is lower for the SiC substrate. This is due to the higher X-ray absorption of SiC relative to Si, which decreases the incident energy into the Au absorber.

Choice of substrate and absorber material

Table 2 shows that there are some material combinations for which the thermoelastic effects are relatively low, in particular the diamond–Au structure at 10-Å irradiation. Similarly, the SiC–W mask structure offers somewhat lower stresses than Si–Au at 10-Å irradiation.

The results presented in Table 2 indicate that in order to reduce the thermoelastic effects, it is advantageous to match the thermal expansion of the mask substrate with the thermal expansion of absorber materials of high thermal conductivity and low Young's modulus relative to the substrate.

II. Mask irradiation with synchrotron storage ring

In X-ray lithography systems utilizing a scanning beam from a synchrotron storage ring as a light source, the dimensional stability of X-ray masks is also an area of concern for high-resolution X-ray lithography. This is because the high radiation doses required to expose conventional resists may cause increases in temperature in the mask materials, leading to thermoelastic distortions during resist exposure [7–11]. Thermal expansion can release the initial intrinsic tensile stress in the mask membranes, resulting in distortion of the pattern. The corresponding intrinsic relative strain of X-ray membranes is usually of the order of 10^{-4}–10^{-5}. For a Si membrane, for instance, tension release requires

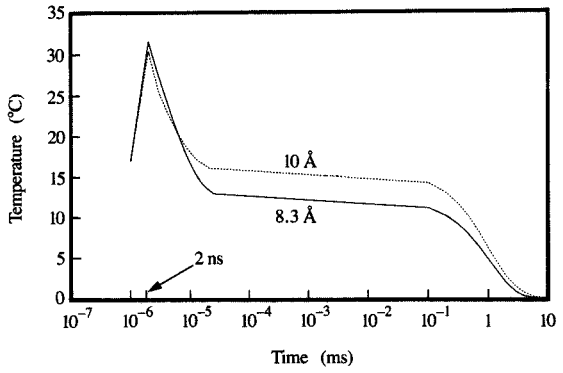

Figure 16

Temperature vs. time calculated at a Au absorber feature of a Si–Au mask where the rise in temperature was maximum. Results are shown for a Si–Au X-ray mask irradiated with 2-ns X-ray pulses of two different wavelengths.

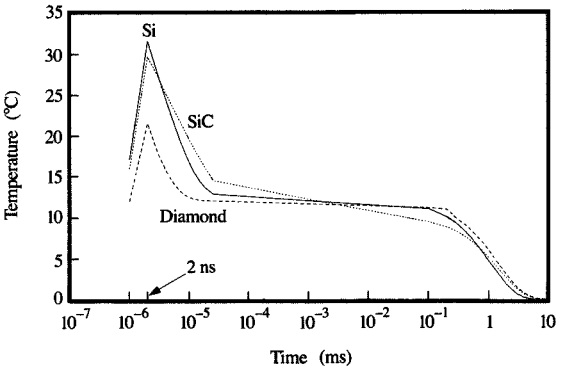

Figure 17

Maximum rise in temperature vs. time at Au absorber on X-ray masks of three different substrate materials.

a temperature increase of 30–100°C. Significant mask distortions may actually occur for much lower temperature increases, as described below.

A synchrotron storage ring emits an intense, narrow fan of radiation. As shown in **Figure 18**, this fan of X-ray radiation is scanned along the Y axis on the mask to expose the desired wafer area. For X-ray exposures in a storage-ring system, the mask is subjected to localized heating by a scanning beam of an effectively finite width.

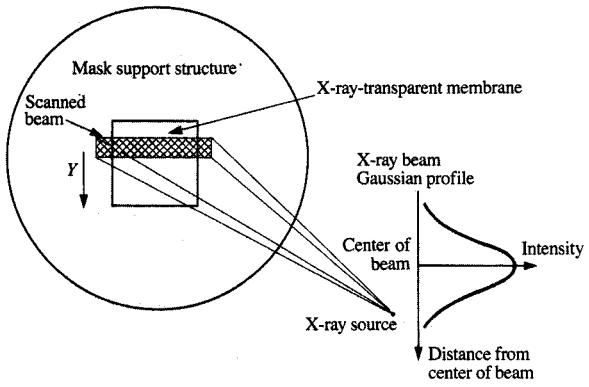

Figure 18

Model for storage-ring irradiation of X-ray mask.

The hot strip on the membrane produced by the absorbed X-ray energy causes a maximum displacement close to the edges of the membrane. The magnitude of this displacement [10] is less than $\delta_{max} = \alpha T_{max} (2\sigma_T) =$ 30 nm for a Gaussian-shaped temperature distribution with $T_{max} = 1°C$ and $\sigma_T = 5$ mm (the thermal expansion coefficient $\alpha = 3 \times 10^{-6}/°C$). If it is assumed that all the absorbed X-ray energy (for example, 100 mW/cm^2) is converted into heat, and also that the thermal properties of the membrane are the same as for the bulk material, the temperature increase in vacuum is expected to be of the order of 30°C. In a He atmosphere, the increase will be less than 1°C. The above estimate indicates that mask distortions may be too high if the X-ray exposures take place in vacuum and are tolerable, but not negligible, in a He atmosphere. Nevertheless, there is at present no experimental evidence that the predicted high temperatures are in fact taking place. The experimental results presented below are expected to shed some light on this issue.

• *Mask-temperature measurements*

The measurement of the temperature distribution in an X-ray mask is not a simple task. Most commonly used techniques involve radiometers and infrared cameras [12, 13]. However, these techniques require knowledge of the thermal emission properties of the membranes. It has been reported [13] that the value of emissivity for a membrane may be quite different from that of the same material in bulk form; in addition, the thermal radiation process may be influenced by interference effects of the emitted radiation in the film and by changes of electrical conductivity with temperature. To overcome these limitations, a technique was developed to measure the temperature of thin membranes using metal resistors on the membrane surface [6].

• *Metal resistors as temperature sensors*

A set of metal resistors was fabricated in the central region (5 mm × 10 mm) of a Si X-ray mask. Gold resistors 50 nm thick were placed on a 1.5-μm-thick intermediate insulating layer of PI, to avoid contact with the heavily doped, conductive Si substrate. The resistor

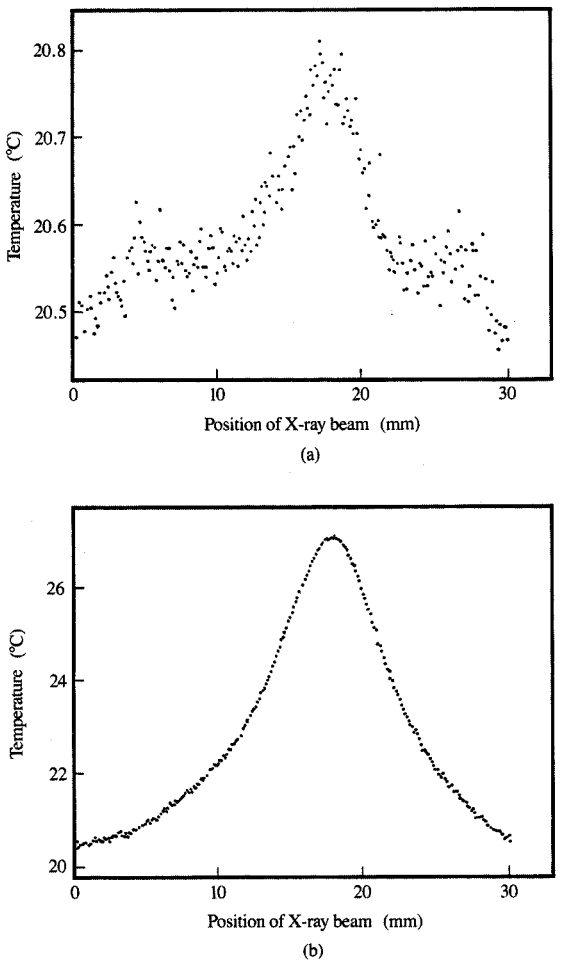

Figure 19

Temperature rise profile at the center of the mask during X-ray beam scanning, for (a) 35-μm mask–wafer gap, 20 torr of He; (b) 25-mm mask–wafer gap, in vacuum. Incident power distribution parameters: maximum — 55 mW/cm^2, standard deviation (width) — $\sigma_p = 2.5$ mm.

pattern was fabricated by optical lithography and wet etching. The etched resistors were covered with an organic layer ≃1 μm thick. Each resistor consists of a serpentine 4 mm long and 10 μm wide, covering a rectangular area measuring 0.5 mm × 2 mm. These gold resistors have a resistivity of 6500 Ω at room temperature, which increases linearly from room temperature to 100°C with a slope of 20 Ω/°C. The sensitivity and response time of the measuring system are of the order of 0.02°C and 1 ms, respectively. The measured thermal time constant for the membrane in vacuum with a 25-mm mask–wafer gap is 230 ± 70 ms.

• *Experimental results (temperature measurements)*
A boron-doped Si membrane 2.5 μm thick was used as a mask substrate with a set of eight resistors fabricated near the center of the membrane [6]. The mask–wafer assembly, with a preset gap, was scanned through the X-ray beam from the storage ring at the rate of 0.01 cm/s. Temperature readings were recorded by an eight-channel data-acquisition system. All eight resistors were sampled within an interval of ≃100 ms. The rise in temperature was analyzed for gap settings of 25 mm and 35 μm, both in vacuum and in a low-pressure helium atmosphere of 20 torr. The temperature profiles measured at the center of the mask (as the beam is scanned along the mask) for 20 torr He and a 35-μm gap are shown in **Figure 19(a)**. Results in vacuum with a 25-mm gap are presented in **Figure 19(b)**. The temperature rise measurements for all four situations are shown in **Figure 20**.

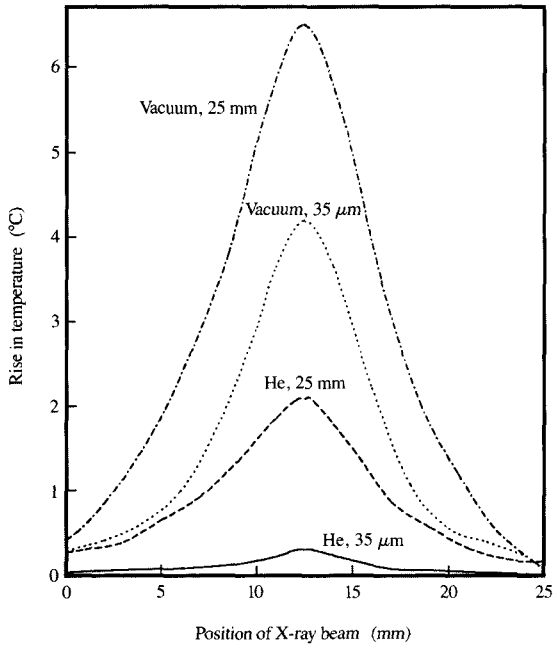

Figure 20

Temperature rise profiles at the center of the mask during X-ray beam scanning.

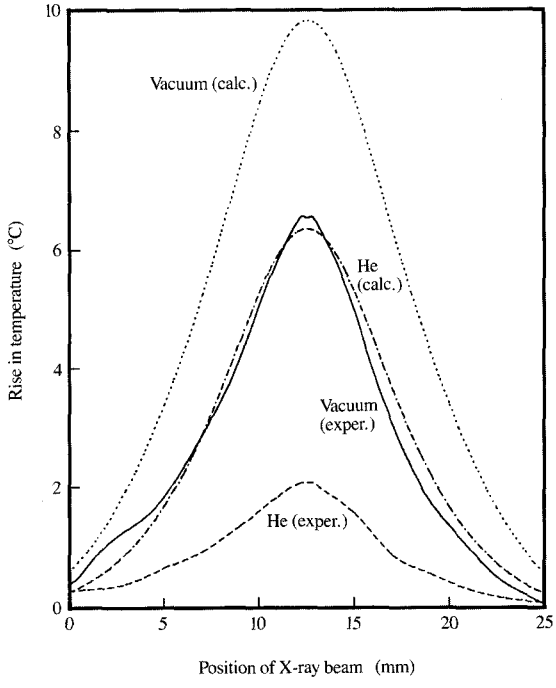

Figure 21

Comparison of experimental and calculated results. Absorbed power distribution parameters: maximum — 30 mW/cm^2, standard deviation — σ_P = 2.5 mm.

The temperature measurements performed by this technique were compared with calculations based on a one-dimensional model [14]. The results of the calculations and the experimental values for the rise in temperature are shown in **Figure 21** and in **Table 3** for vacuum and 20 torr He atmosphere. The parameters of the power density distribution absorbed in a 25-mm-square membrane were P_{abs} = 30 mW/cm^2 and σ_P = 2.5 mm.

There is no good agreement between the measurements and the calculations, especially for the vacuum environment. In this case the rise in temperature is expected to be 25°C, independent of the mask–wafer gap. The experimental values are significantly lower and gap-dependent, as shown in Table 3. The calculations show that the mask thermal conductivity is responsible

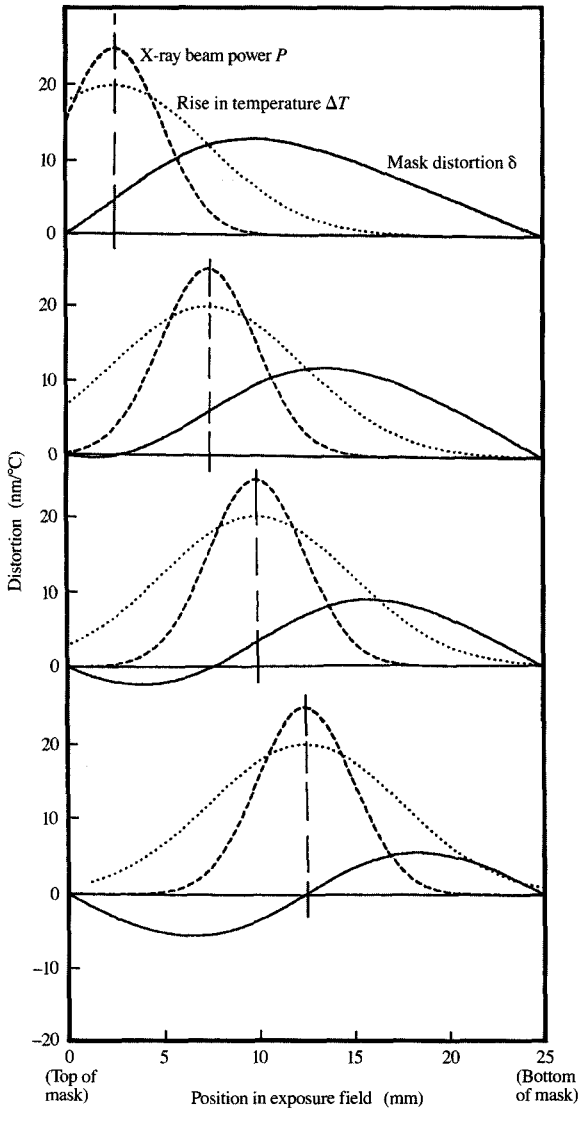

Figure 22

Calculated mask thermoelastic distortions for different X-ray beam positions. Calculations were made for a 25-mm-wide Si mask, thermal expansion coefficient — $\alpha = 2.6 \times 10^{-6}$/°C, $\nu = 0.25$, standard deviation for incident power — $\sigma_P = 2.5$ mm, standard deviation for temperature distributions — $\sigma_T = 5.0$ mm.

for only a few percent of the energy losses. However, it significantly reduces the maximum rise in temperature (see Table 3), because it causes a more even distribution of the thermal energy over the mask surface, in this way enhancing the radiation losses. The discrepancies shown in Table 3 for a large gap may be explained by assuming

Table 3 Maximum rise in temperature (°C) in X-ray mask.

ΔT_0	*Vacuum*		*20 torr He*	
	25-mm gap	*35-μm gap*	*25-mm gap*	*35-μm gap*
Calculated*	25	25	13	0.07
Calculated†	9.7	9.7	6.3	0.07
Measured	6.6	4.1	2.1	0.3

†With and *without membrane thermal conductivity.

different thermal parameters for the mask materials. It has been suggested [15] that temperature increases and thermal loads for the optical components used to shape synchrotron radiation are overestimated when conventional calculation methods and material properties are utilized. The experimental results presented above support this statement. On the other hand, for a low-pressure helium atmosphere and a 35-μm gap, the measured value of 0.3°C is higher than the calculated one of 0.07°C. The latter results are not well understood and may be attributed to our inability to determine the actual helium pressure inside the gap.

• *Model of thermoelastic distortions*

In this section a new, one-dimensional model and experimental results are presented that relate thermoelastic distortion of the mask during X-ray beam scanning to the blurring and displacement of the printed image [6].

When the X-ray beam with strip-like cross section (see Figure 18) is moving in the Y direction, the absorbed energy produces a hot strip on the membrane, with a temperature distribution $T(y)$, where y is the position on the membrane in this one-dimensional model. The rise in temperature $\Delta T(y, Y)$ at y for each position Y of the beam will induce in the mask distortions $\delta(y, Y)$, which depend on the thermal expansion coefficient α and the Poisson ratio ν of the material:

$$\delta(y, Y) = \alpha(1 + \nu) \int_0^y \Delta T(\xi - Y, Y)d\xi - \alpha(1 + \nu) \frac{y}{L} \int_0^L \Delta T(\xi - Y, Y)d\xi, \quad (1)$$

where L is the length of the membrane. This expression is the solution of the following thermoelastic equation [16] reduced to a one-dimensional case [17] for a plane strain–stress state,

$$\frac{\partial^2 \delta}{\partial y^2} = \alpha(1 + \nu) \frac{\partial \Delta T}{\partial y},$$

with the boundary conditions corresponding to zero

displacement at the edges of the membrane: $\delta(0, Y) = \delta(L, Y) = 0$. As an approximation, the Poisson ratio in this paper was taken to be $\nu = 0.25$ for Si and boron nitride. An expression similar to Equation (1) was obtained in [9], but without the factor $(1 + \nu)$.

Another special situation occurs when there is a uniform temperature distribution over a whole mask: $\Delta T(y, Y) = T_c$. Then there is no distortion:

$$\delta = \alpha(1 + \nu)\left(T_c y - \frac{y}{L} T_c L\right) = 0.$$

Figure 22 illustrates the mask distortion for different positions of the X-ray beam on the mask. When the beam is positioned close to the top edge of the mask, all the points on the mask shift down. As the beam moves down the mask, the direction of the displacement for the points near the top edge of the mask changes: The points shift to the top. And when the beam is at the center of the mask, all the displacements are directed toward the edges (outward). Similar behavior can be observed when the beam is located below the mask center. In this case, the directions of the displacements are reversed relative to the case above. The above description indicates that during beam scanning, the mask distortions are not fixed, but all the points on the mask move back and forth in the plane of the mask. It is expected that an image from the mask printed on the wafer will reflect this movement. During exposure with a scanning beam, each point on the mask is projected to a slightly different place on the wafer, and the printed image depends on the average position of each point on the mask, weighted according to the X-ray beam energy distribution $P(Y)$. The shift of the printed features $\delta_{im}(y)$ is given by

$$\delta_{im}(y) = \langle \delta(y) \rangle = \frac{\int_{-A}^{A} \delta(y, Y) P(y - Y) dY}{\int_{-A}^{A} P(y - Y) dY},$$

where $2A$ is the scanning range.

Useful approximate expressions of the distortions of the printed image can be obtained for the area of the exposure field relatively far from the edges,

$$\delta_{im}(y) \cong \alpha(1 + \nu)\Delta T_0 \sigma_T \left(1 - \frac{2y}{L}\right),$$

where ΔT_0 and σ_T are the maximum and the standard deviation of the temperature distribution, respectively.

A maximum displacement of

$$\sigma_{im}^{max} \cong \alpha(1 + \nu)\Delta T_0 \sigma_T \left(1 - \frac{3\sigma_T}{L}\right)$$

can be expected for the positions in the exposure field given by $y = 1.5\sigma_T$ and $y = L - 1.5\sigma_T$. In addition to being displaced, the feature edges of the printed image will be smeared (blurred). Presented in terms of the standard deviation (RMS), the edge blur is given by the expression

$$\sigma_{blur}(y) = \sqrt{\langle \delta^2(y) \rangle - \langle \delta(y) \rangle^2}.$$

The maximum value of the blur, which occurs at the center of the exposure field, can be estimated using the expression

$$\sigma_{blur}^{max} = \alpha(1 + \nu)\Delta T_0 \frac{\sigma_P \sigma_T}{\sqrt{\sigma_P^2 + \sigma_T^2}},$$

which also includes a parameter for the X-ray beam intensity distribution σ_P. For a 25-mm Si membrane with thermal expansion coefficient [18] $\alpha = 2.6 \times 10^{-6}$/°C and with temperature and X-ray beam distribution parameters $\sigma_T = 5$ mm, $\sigma_P = 2.5$ mm, we obtain numerical values for maximum displacement $\delta_{im}^{max} = 6.5$ nm/°C and for blur $\sigma_{blur}^{max} = 7.2$ nm/°C.

The phenomena described above are shown in **Figure 23**. From the analysis, we find that all the displacements

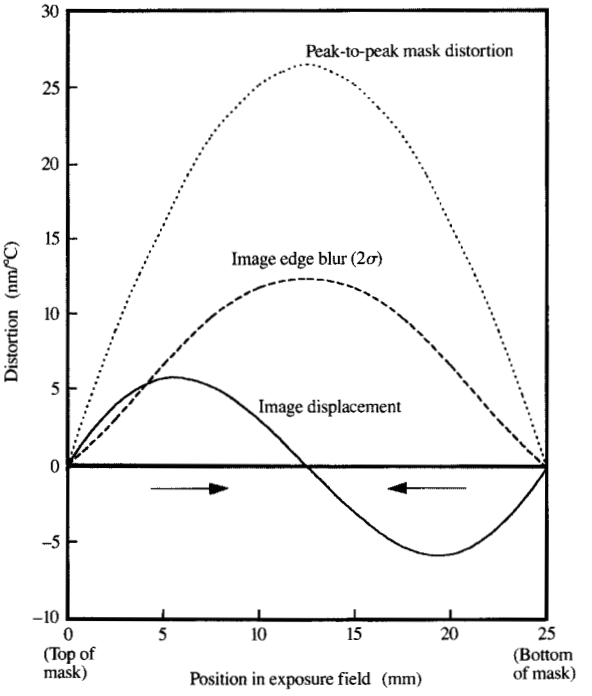

Figure 23

Calculated thermoelastic distortions of the printed image. Parameters are the same as in Figure 22. Note that all the displacements are directed inward.

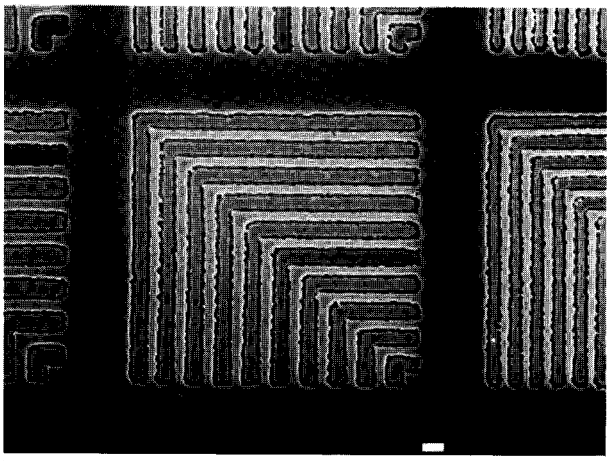

(a)

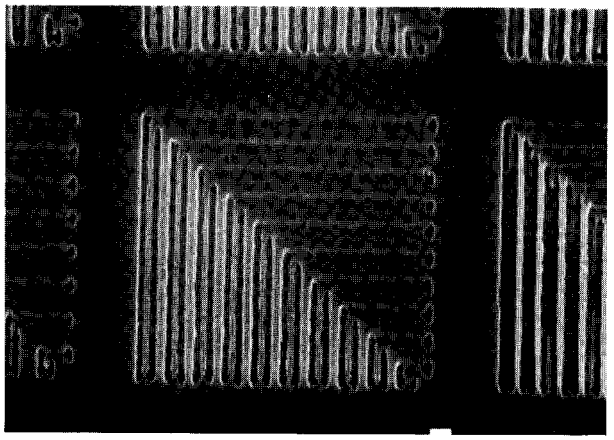

(b)

Figure 24

Thermoelastic printed image blur: (a) image printed at 20 torr of He; (b) image printed in vacuum. Boron nitride mask obtained from University of Wisconsin. Maximum X-ray intensity — 80 mW/cm^2, mask–wafer gap 30–40 μm. Beam scanned in vertical direction.

in the printed image are directed inward: The image actually shrinks in a nonlinear fashion while the mask expands. Moreover, the movement of the feature during exposure should manifest itself in a smearing of the feature edges—thermoelastic blur—with a magnitude 2σ, as shown in Figure 23. For comparison, peak-to-peak mask distortions are given on the same plot.

• *Experimental results (thermoelastic distortion)*
In order to experimentally study thermal distortion of printed images, several X-ray masks with different patterns were printed on wafers coated with PMMA resist, using the X-ray radiation from the storage ring (Alladin, 800 MeV, 2.08-m radius) at the University of Wisconsin [6].

A mask–wafer assembly with a gap of 30–40 μm was scanned through the narrow X-ray beam (with cross section 5 mm × 30 mm). The power density was maintained at typical X-ray lithography levels of about 80 mW/cm^2. Slow scanning rates of $\simeq$1 cm/min were chosen, to provide quasistatic exposure conditions and exposure doses of 3 J/cm^2.

For the studies of the thermoelastic-blur effect, chevron-type patterns were used on a boron nitride membrane 75 mm in diameter. The feature sizes varied from 0.7 μm to 3.5 μm. During printing, the direction of the scan was parallel to one set of lines in the chevron pattern and perpendicular to the other set. Scanning electron microscope (SEM) micrographs of the resist images of the chevron patterns printed in a low-pressure He atmosphere are shown in **Figure 24(a)** and for vacuum in **Figure 24(b)**. The beam was scanned in the vertical direction. The quality of the edges of the lines in the image exposed in helium does not depend on the direction of the X-ray beam scan. The slightly rough edges reflect imperfections of the image on the mask. The experiments conducted in vacuum clearly reveal a smearing effect: The lines perpendicular to the scan are blurred, while those oriented along the direction of the scan are well-defined and smooth. To corroborate the above results, a second set of exposures was made after the mask was rotated 90° (to change the orientation of the lines printed in the first set of experiments). In both experiments, the wafers were slightly underdeveloped in order to emphasize the line profile of the printed image. The results of both sets of exposures were identical. An estimate of the smearing effect made with our model predicts a value of $2\sigma = 0.25$ μm, which is comparable to the SEM observations shown in Figure 24(b). (For the estimate, the following assumptions were made: a maximum rise in temperature of $\Delta T_0 = 25$°C on the mask, with absorbed maximum power 50 mW/cm^2 and $\sigma_P = \sigma_T = 2.5$ mm; $\alpha = 2.2 \times 10^{-6}$/°C was taken from [4].)

To measure the shift of the features in the printed image, a boron-doped Si X-ray mask with an array of crosses was used. The positions of the crosses on the mask and wafers were measured with a NIKON[3] 2I tool. The measurements performed on the wafers exposed in He did not reveal appreciable shifts. This was expected from the measured rise in temperature on the mask, which was about $\Delta T_0 = 0.3$°C (see Table 3). Smearing of the edges of the pattern printed in vacuum would have allowed detection of shifts exceeding 0.2 μm. For a 25-mm Si membrane, this shift corresponds to a temperature increase of the order of $\Delta T_0 \simeq 35$°C, which is significantly higher than the temperatures observed in all our measurements in vacuum.

[3] NIKON is a trademark of Nikon Corporation, Tokyo, Japan.

Nevertheless, thermoelastic distortions have been observed by other authors [19–21]. One of the papers reported measurements of the distortion of the printed image [20] obtained from a mask with a polyimide membrane (see **Table 4**). In those experiments, the thermoelastic distortions were noticeable, since the thermal expansion coefficient of polyimide films [10, 19] is about ten times higher than the corresponding value for silicon. The author [20] estimates a maximum rise in the temperature distribution of $\Delta T_0 \simeq 40°C$ for his experimental conditions. The results of calculations with our model with a $\Delta T_0 = 40°C$ rise in temperature are given in Table 4.

We observe that with the 40°C rise in temperature, the calculated shifts differ appreciably from the measurements reported in [20]. The table also shows good agreement between the experimental values [20] and the results predicted by the model using an increase in temperature of $\Delta T_0 = 10.6°C$ as a fitting parameter. In view of the results of the temperature measurements presented in this paper, the lower temperature value (10.6°C) required to fit the quoted experimental data appears reasonable. The following data were used for the calculations: thermal expansion coefficient of polyimide [4] $\alpha = 23 \times 10^{-6}$ and Poisson ratio $\nu = 0.40$; mask membrane size [20] $L_M = 50$ mm, half-width of the X-ray beam intensity and temperature distributions [20] $\Gamma_{1/2} = 7$ mm.

Table 4 Thermoelastic image distortions.

Position of X-ray beam, Y (mm)	*Calculated values using* $\Delta T_0 = 40°C$ (μm)	*Values reported in [20]* (μm)	*Calculated values using* $\Delta T_0 = 10.6°C$ (μm)
25.0	0.0	0.0	0.0
15.0	2.99	0.70	0.79
5.0	1.04	0.38	0.28
0.0	0.0	0.0	0.0
−5.0	−1.04	−0.32	−0.28
−15.0	−2.99	−0.63	−0.79
−25.0	0.0	0.0	0.0

Conclusions

In Part I of this paper, results of computer calculations of thermoelastic effects on several mask structures are presented. Commercially available finite element computer codes were used. The results indicate that it is possible to obtain some reduction in the magnitude of the thermoelastic effects by proper selection of the substrate and absorber materials and the system operating wavelength. In particular, for pulsed X-ray lithography systems operating at 10 Å, there are some advantages in using X-ray masks of SiC–W, Si–W, or, preferably, diamond–Au. In addition, the calculations show that there is only a modest decrease (about 30%) in the stress in the W absorber of the Si–W structure compared with the stress in the Au absorber in the Si–Au structure. The magnitude of the stress reduction caused by the use of a PI film between the Au and the Si substrate is found to depend on the thermoelastic properties of the particular polyimide film. The results also indicate that the pulse repetition rate can be as high as 100 Hz without causing appreciable heating of the mask, when the exposures are performed in a He atmosphere with a 40-μm gap. The results presented in this paper are conservative, since radiation and other energy-dissipative effects (such as thermally induced sound waves) were not considered in the calculations. However, in some cases it was found that the calculated maximum stress values were comparable to the values of the materials' intrinsic stress. This indicates that when powerful X-ray sources become available (with X-ray pulse amplitudes similar to the one used in these calculations—about 10 mJ/cm^2), there will be need for experimental determination of the maximum thermoelastic effects and thermal cycling of the mask substrate and absorber materials from the point of view of mask distortion and lifetime (fatigue).

For the case of X-ray irradiation with a storage ring, presented in Part II, a technique was developed for temperature measurements on thin membranes by the use of built-in metal resistors. Using this technique, we determined the rise in temperature in an X-ray mask under realistic operating conditions, with a 35-μm mask–wafer gap. The experimental results using the resistor probes differ from the calculations, showing a significantly lower rise in temperature in vacuum and a higher rise in temperature in helium. More work is required to understand these results fully.

A new feature of thermoelastic distortion during X-ray beam scanning—a smoothing effect in the printed image—was recognized and modeled. The predicted distortions of the printed image are significantly smaller than the pattern distortions on the mask during exposure, and are directed inward (toward the center of the exposure field). The relatively small distortion values on the printed image result from the averaging effect of beam scanning. In addition, the model predicts a small magnitude for the blur of the edges of the printed features.

Finally, the experimental results on thermoelastic distortion agree with the predictions and show that the effects are detectable in SEM observations when the mask–wafer assembly is operated in vacuum. However, the effect is negligible for operation in a low-pressure He atmosphere, as is planned for X-ray lithography systems.

Acknowledgments

The authors would like to thank the X-ray lithography groups at Yorktown and East Fishkill for fruitful interactions and for the comments and support of Alan Wilson, Ajay Sharma, and Michael Wesley. We also thank R. Fair for NIKON 2I measurements. The experimental results presented in Part II were obtained at the Madison Wisconsin Center of Excellence for X-Ray Lithography under the leadership of Franco Cerrina. We would like to thank O. Vladimirsky, M. Hansen, R. Nachman, and G. M. Wells for technical assistance with the experimental results. Also, we would like to acknowledge the support of the Defense Advanced Research Projects Agency in conjunction with the National X-Ray Lithography Program.

References

1. J. R. Maldonado, "X-Ray Lithography, Where It Is Now, Where It Is Going," *J. Electron. Mater.* **19,** 699–709 (1990).
2. A. Ballantyne, H. Hyman, C. L. Dym, and R. Southworth, "Response of Lithographic Mask Structures to Intense Repetitively Pulsed X-Rays: Thermal Stress Analysis, and Dynamic Response Analysis," *J. Appl. Phys.* **58,** 4717–4729 (1985).
3. H. A. Hyman, A. Ballantyne, H. W. Friedman, D. A. Reilly, R. C. Southworth, and C. L. Dym, "Intense-Pulsed Plasma X-ray Sources for Lithography: Mask Damage Effects," *J. Vac. Sci. Technol.* **21,** 1012–1016 (1982).
4. I. Shareef, D. Katcoff, and J. R. Maldonado, "Thermal and Mechanical Model of X-Ray Lithography Masks Under Short Pulse Irradiation," *J. Vac. Sci. Technol. B* **7,** 1575–1582 (1989).
5. I. Shareef, J. R. Maldonado, and D. Katcoff, "Thermoelastic Effects in X-Ray Lithography Masks Under Pulse Irradiation," *Proc. Microcirc. Eng. 10* (1990).
6. Y. Vladimirsky, J. R. Maldonado, R. Fair, R. Acosta, O. Vladimirsky, R. Viswanathan, H. Voelker, F. Cerrina, G. Wells, M. Hansen, and R. Nachman, "Thermal Effects in X-Ray Masks During Storage Ring Irradiation," *J. Vac. Sci. Technol. B* **7,** 1657–1661 (1989).
7. W. D. Grobman, "Synchrotron Radiation X-Ray Lithography," *Handbook on Synchrotron Radiation*, E.-E. Koch, Ed., North-Holland Publishing Co., Amsterdam, Netherlands, 1983, pp. 1131–1165.
8. A. Heuberger, "X-Ray Lithography," *Proc. Microcirc. Eng.* **5,** 3–38 (1986); *J. Vac. Sci. Technol. B* **6,** 107–121 (1988).
9. K. Heinrich, H. Betz, and A. Heuberger, "Heating and Temperature Induced Distortions of Silicon X-Ray Masks," *J. Vac. Sci. Technol. B* **1,** 1352–1357 (1983).
10. M. Karnezos, R. Ruby, B. Heflinger, H. Nakano, and R. Jones, "An Alternative to Gold for X-Ray Masks," *J. Vac. Sci. Technol. B* **5,** 283–287 (1987).
11. M. Karnezos and P. Weimar, "X-Ray Mask Heating During Electron-Beam Patterning," *J. Vac. Sci. Technol. B* **5,** 278–282 (1987).
12. I. Mori, H. Komano, M. Hori, Y. Kikuchi, Y. Horiike, and K. Tanaka, *Photon Factory Activity Report 1987,* No. 5, Osaka University, Osaka, Japan, 1987, p. 312.
13. Darii Ya. Svet, *Thermal Radiation*, Consultant Bureau, New York, 1965.
14. Y. Vladimirsky, J. Maldonado, O. Vladimirsky, F. Cerrina, M. Hansen, and R. Nachman, "Thermoelastic Effects in X-Ray Masks During Storage Ring Irradiation," *Proc. Microcirc. Eng.* **10** (1990).
15. B. P. Youngman, "History of Thermal/Stress Analysis Method Used at Stanford Synchrotron Radiation Laboratory," *Nucl. Instr. & Meth. in Phys. Res. A* **266,** 525–530 (1988).
16. Heinz Parkus, *Thermoelasticity*, Blaisdel Publishing, Waltham, MA, 1968, Ch. 3, pp. 24–29.
17. William A. Day, *Heat Conduction Within Linear Thermoelasticity*, Springer-Verlag, New York, 1985, Ch. 2, p. 6.
18. *Thermophysical Properties of Matter, Vol. 13*, Y. S. Touloukian, Ed., IFI/Plenum, New York, 1977, p. 154.
19. J. R. Schneider and P. Tischer, *Siemens Forsch.-u. Entwickl.-Ber.* **12,** 306–312 (1983).
20. K.-H. Müller, *Proc. Microcirc. Eng. '83,* 261–268 (1983).
21. R. Ruby, D. Boldwin, and M. Karnezos, "The Use of Diffraction Techniques for the Study of In-Plane Distortions of X-Ray Masks," *J. Vac. Sci. Technol. B* **5,** 272–277 (1987).

Received February 20, 1990; accepted for publication July 16, 1990

Iqbal A. Shareef *IBM Research Division, Thomas J. Watson Research Center, P.O. Box 218, Yorktown Heights, New York 10598.* Mr. Shareef is an advisory engineer in the Manufacturing Research Department at the IBM Thomas J. Watson Research Center. He received his B.S from Osmania University, Hyderabad, India, in 1975 and his M.S in mechanical engineering from the University of Illinois at Urbana-Champaign in 1981. Mr. Shareef joined IBM at East Fishkill in 1981, working on optical lithography, and then moved to the thermal technology development area in 1983. Since joining IBM Research in 1989, he has been involved with finite element modeling techniques.

Juan R. Maldonado *IBM General Technology Division, Route 52, Hopewell Junction, New York 12533.* Dr. Maldonado received a Doctorate degree in Ciencias Físico Matemáticas from the University of Havana in 1961, and a Ph.D. in experimental solid state physics in the field of superconductivity from the University of Maryland in 1968. That same year he joined Bell Laboratories, Murray Hill, NJ, where he worked in the fields of ferroelectric ceramics, electro-optic display devices, and liquid crystals, and in the 1970s pioneered work in X-ray lithography with co-workers. Dr. Maldonado joined IBM in 1980 at the Thomas J. Watson Research Center in Yorktown Heights, NY, where he was manager of the X-Ray Lithography Processes group until 1988. Since then, he has worked at the Advanced Technology Center in East Fishkill, and has been involved with the transfer of X-ray lithography technology from IBM Research to the future Advanced Lithography Facility (ALF). Dr. Maldonado has published over 60 papers and two book chapters in the above-mentioned fields; he holds more than a dozen patents assigned either to Bell Laboratories or to IBM. He is a member of the American Physical Society, IEEE, AAAS, and Sigma Xi.

Yuli Vladimirsky *IBM General Technology Division, Route 52, Hopewell Junction, New York 12533.* Dr. Vladimirsky received his M.S. in the physics of metals in 1964 and his Ph.D. in physics and mathematics in 1970 from the Leningrad Polytechnic Institute. After completing his studies, Dr. Vladimirsky conducted research on defects, radiation damage, X-ray luminescence, and other irradiation effects in solids, and experimental and theoretical investigations in X-ray optics, mosaic structure, and X-ray optical properties of crystals and pseudo-crystals. As a Visiting Professor, he lectured at the Leningrad State University and Leningrad Polytechnic Institute on X-ray diffraction theory and X-ray optics, and on the theory of probability and statistics. From 1981 to 1984 Dr. Vladimirsky was a Visiting Scientist at the IBM Thomas J. Watson Research Center and worked on research and development of submicron photo-, X-ray, and electron-beam lithography techniques for fabrication of deep UV and soft X-ray optical elements. From 1984 until 1988 he was a Research Scientist at the Center for X-Ray Optics, Lawrence Berkeley Laboratory, University of California, working with the Nanostructure Fabrication group at the IBM Thomas J. Watson Research Center on the development of imaging optics for soft X-ray synchrotron radiation. Dr. Vladimirsky joined IBM at East Fishkill in 1988 and is currently working on the physical aspects of imaging in X-ray lithography, including thermoelastic and diffraction phenomena. He is a member of the American Physical Society.

David L. Katcoff *IBM General Technology Division, Essex Junction, Vermont 05452.* Mr. Katcoff received a B.S. in chemistry from Columbia University in 1973, an M.B.A. from the Columbia Graduate School of Business in 1975, and an M.S. in physics from the University of Connecticut in 1987. He is a senior associate engineer at IBM Burlington, currently working in device modeling.